Fig. 1　神経変性疾患はコンフォメーション病である．
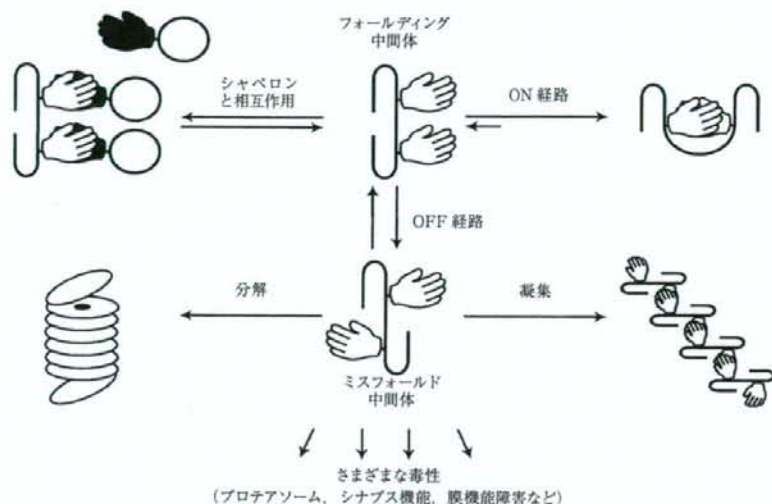

Fig. 2　タンパク質のフォールディングと凝集形成：タンパク質のフォールディングの効率率は ON
経路に乗って Native な構造をとる割合によって決まる．正しくフォールディングされなかったタ
ンパク質は OFF 経路をたどってミスフォールド中間体となり，ユビキチンプロテアソーム系に
よって分解される．しかし分解を逃れると，non-native なオリゴマー，線維形成につながる凝集形
成をおこなう．

けによってひきおこされるだけでなく，ミスフォールドタン
パク質の毒性から自らを守るために細胞が自ら凝集体を形成
する仕組みがあることが明らかになり，アグレソーム（aggre-
some）と名づけられた[4]．
　ミスフォールドタンパク質はその物理化学的特性のみなら
ず，生体防御反応をひきおこすことによって毒性を発揮する．
その代表となるのが，小胞体ストレス応答である．小胞体は分
泌系タンパク質のフォールディングを助け，品質管理をおこ
なう細胞内小器官であるが，その機能が破綻し，過剰にミス
フォールドタンパク質が蓄積した状態が小胞体ストレスであ
る．生体はミスフォールドタンパク質を取り除くために小胞

Table 1　Take Home Message

・神経変性疾患は異常構造のミスフォールド蛋白質の蓄積
　によるコンフォメーション病である．
・ミスフォールド蛋白質はアミロイド線維を形成する．
・ミスフォールド蛋白質の毒性は蛋白質そのもの and/or そ
　れに対する生体反応によるらしい．
・非細胞自律性（non-cell-autonomous）細胞死の存在が示さ
　れた．
・治療法開発はミスフォールド蛋白質を減少させることを
　目標にすすめられている．

体シャペロンの転写亢進をはじめとしてさまざまな手段を講
じるが，ミスフォールドタンパク質の排除に失敗したばあい

には，アポトーシスで死んでしまう．このようなメカニズムが家族性パーキンソン病や白質ジストロフィーで提唱されている[5].

4. 神経変性の新たなパラダイムと今後の課題

　神経変性疾患の動物モデルの成功とともに，新たに細胞間相互作用，あるいはシステムの立場から神経変性をとらえる考え方が登場した．上記のミスフォールドタンパク質の毒性のメカニズムはいずれも神経細胞内に異常蛋白質が蓄積することによって，細胞の内側から細胞死をひきおこすとの前提に立ったものであった．ところが，家族性 ALS のモデルのよいモデルとなる，運動ニューロンが選択的に変性する変異 SOD1 トランスジェニックマウスの研究によって，同じく変異タンパク質を発現する周囲のアストログリアやミクログリアによって，神経細胞死が誘発される，非細胞自律性（non-cell autonomous）細胞死が運動ニューロンの変性に重要な役割を担っていることが明らかになった[6]．これにはアストロサイトの分泌する液性因子や炎症がかかわっている可能性がある．

　また同じく変異 SOD1 が分泌されて，細胞外から毒性を発揮するとの報告も出されており，細胞死への細胞外からの因子の関与の注目が高まっている[7].

　今後の課題としては，さまざまな機構を毒性をひきおこすミスフォールドタンパク質を除去する治療法の確立が急務であり，RNAi やワクチンをもちいた治療法の可能性が模索されている[8]（Table 1).

文　献

1) 金澤一郎：変性疾患．神経内科学第 2 版，豊倉康夫　編，朝倉書店，2004, pp 458—547
2) Ross CA, Poirier MA: Protein aggregation and neurodegenerative disease. Nat Med 2004; 10 Suppl: S10—17
3) Carrell RW, Lomas DA: Conformational disease. Lancet 1997; 350: 134—138
4) Kopito RR: Aggresomes, inclusion bodies and protein aggregation. Trends Cell Biol 2000; 10: 524—530
5) Imai Y, Soda M, Inoue H, et al: An unfolded putative transmembrane polypeptide, which can lead to endoplasmic reticulum stress, is a substrate of Parkin. Cell 2001; 105: 891—902
6) Boillée S, Yamanaka K, Lobsiger CS, et al: Onset and progression in inherited ALS determined by motor neurons and microglia. Science 2006; 312: 1389—1392
7) Urushitani M, Sik A, Sakurai T, et al: Chromogranin-mediated secretion of mutant superoxide dismutase proteins linked to amyotrophic lateral sclerosis. Nat Neurosci 2006; 9: 108—118
8) Saito Y, et al: Transgenic siRNA halts ALS in a mouse model. J Biol Chem 2005; 280: 42826—42830

Abstract

Recent progress and future direction of neurodegenerative disease research

Ryosuke Takahashi, M.D., Ph.D.
Department of Neurology, Kyoto University Graduate School of Medicine

　　Although the pathogenetic mechanisms underlying neurodegenerative diseases have been long elusive, recent progress in molecular neurogenetics and neurobiology has suggested that accumulation of misfolded protein leads to dysfunction and degeneration of neurons. Misfolded proteins have propensities to form fibrils termed amyloid fibrils. In the process of amyloid fibrils, intermediate forms such as oligomers and protofibrils are produced and thought to have cytotoxic effects to neurons. Neurotoxicity mediated by misfolded proteins are also caused by stress response such as unfolded protein response. Moreover, recent findings indicate that non-neuronal cells surrounding neurons or extracellular misfolded proteins promote neurodegeneration. To eliminate toxic proteins would constitute promising future therapy for neurodegenerative disorders.

(Clin Neurol, 48: 903—905, 2008)

Key words: Conformational disease, misfolded protein, oligomer, endoplasmic reticulum (ER) stress, non-cell autonomous

ゲノム医学

京都大学大学院医学系研究科脳病態生理学講座臨床神経学（神経内科）教授

高橋良輔

　神経変性疾患の定義は教科書では「徐々に発症し，緩徐だが常に進行する神経症状を呈し，その症状も多くは対称的に，ある種の系統がおかされ(systemic disease)，家族性のことが多い(heredo-degenerative disease)ものであり，一方，病理学的には，特に神経細胞を中心とするさまざまな種類の退行性変化があり，血管障害，感染，中毒などの明らかな原因がつかめない一群の神経疾患」とされている(金澤一郎，2004年)．代表的な神経変性疾患には，大脳皮質ニューロンが侵され認知症を発症するアルツハイマー病，中脳黒質ドーパミンニューロンの選択的変性により運動障害を引き起こすパーキンソン病，脊髄運動ニューロンの選択的変性で全身の骨格筋が麻痺する筋萎縮性側索硬化症(amyotrophic lateral sclerosis；ALS)が挙げられる．これらの疾患はいずれも長期にわたって重篤な障害を患者に強いるだけでなく，闘病生活を支える家族など支援者への負荷も多大なものになる．しかも，ほとんどの神経変性疾患に共通するリスクファクターは加齢であり，人口の21％以上が65歳以上の"超高齢社会"を迎えつつあるわが国では，患者数がすでに100万人を超えるアルツハイマー病を筆頭に患者数の増加が確実であるなか，その原因究明とそれに基づく治療法開発は急務といえる．

　上の定義にあるように，神経変性疾患には非遺伝性(孤発性)と遺伝性(家族性)のものがある．脊髄小脳変性症では，多系統萎縮症などを除いて遺伝性が大半を占める一方，アルツハイマー病，パーキンソン病，ALSでは，孤発性のものが大半を占め，家族性のタイプは5～10％を占めるにすぎない．ところが大変興味深いことに，単一遺伝子の異常で起こる家族性疾患のなかには，臨床的にも病理学的にも孤発性疾患とそっくりなものがある．このことから孤発性疾患と家族性疾患は遺伝子レベルで共通の病態をもつと仮定し，家族性疾患を，病因への直接の手がかりを欠く孤発性疾患解明の鍵とみなす考えが生まれた．ポジショナルクローニングの発展により，ほとんどすべての家族性変性疾患の病因遺伝子

神経変性疾患とゲノム

特集にあたって

が同定できるようになると，病因遺伝子の機能解析をもとに，家族性疾患と類似する孤発性疾患への挑戦が始まった．

その結果は今日まで輝かしい成功を収めている．Aβ 蛋白質前駆体や Aβ 蛋白質産生酵素であるプレセニリンの変異がまれな家族性アルツハイマー病の原因になるという発見は，アルツハイマー病の大半を占める孤発性のタイプもまた，Aβ 蛋白質が引き起こす疾患であるという数多くの証拠を生み，Aβ ワクチン療法という治療法の開発にまでつながった．また，世界に数家系しかない家族性パーキンソン病の病因遺伝子として発見された α-シヌクレインは，わが国だけでも 12 万人を数える孤発性パーキンソン病の病因蛋白質としての位置を確立しつつある．このように「まれな家族性疾患から，一般的な孤発性疾患へ」というストラテジーを踏襲し，ALS や多系統萎縮症でも家族性疾患の解明が行われている．また，神経変性疾患は異常蛋白質の蓄積により生じるコンフォメーション病であるとの見方も一般化してきたが，孤発例の患者脳から異常蛋白質の実態が同定されたのちに，その蛋白質の変異で生じる家族性疾患が同定された前頭側頭葉変性症のようなケースも現れた．

一方，孤発性疾患は多くの遺伝子の影響があるという仮定のもと，全ゲノム関連解析も ALS，パーキンソン病などで進められている．驚くべきことにパーキンソン病では，前述の α-シヌクレインが孤発性パーキンソン病の疾患感受性遺伝子として同定されるという成果が得られている．

このように神経変性疾患の病因解明のフロンティアを切り開きつつあるゲノム研究の現状をそれぞれの領域の第一人者の先生方にご紹介いただいた．すべて力のこもった，またわかりやすい総説であり，読者の皆様のお役に立つことを祈っている．

In vivo imaging of microglial activation using a peripheral benzodiazepine receptor ligand: [11C]PK-11195 and animal PET following ethanol injury in rat striatum

Hiroshi Toyama · Kentaro Hatano · Hiromi Suzuki
Masanori Ichise · Sotaro Momosaki · Gen Kudo
Fumitaka Ito · Takashi Kato · Hiroshi Yamaguchi
Kazuhiro Katada · Makoto Sawada · Kengo Ito

Abstract

Objective To investigate whether [11C]PK-11195, a specific peripheral benzodiazepine receptors (PBRs) ligand for positron emission tomography (PET), can show activated microglia in a rat brain injury model.

Methods On day 1, ethanol was injected into the rat's right striatum (ST) using a stereotaxic operative procedure. On day 3, head magnetic resonance imaging (MRI) scans for surgically treated rats were performed to evaluate ethanol injury morphologically. On day 4, dynamic PET scans (17 injured rats and 7 non-injured controls) were performed for 60 min with an animal PET scanner under chloral hydrate anesthesia following a bolus injection of [11C]PK-11195 through tail vein. Because PBRs are present throughout the brain, there is no suitable receptor-free reference region. The reference tissue model may not be applicable because of low target to background ratio for low affinity of [11C]PK-11195 to PBRs. We evaluated the PBRs binding with regions of interest

(ROIs)-based approach to estimate total distribution volume (V). We used an integral from 0 min to 60 min (V_{60}) as an estimate of V. On the coronal PET image, ROIs were placed on bilateral ST. Differences in right/left ST V_{60} ratios between lesioned and unlesioned control rats were compared using unpaired t tests. Immunohistochemical staining was performed for confirming the presence of activated microglia following decapitation on the PET experiment day.

Results The right/left ST V_{60} ratios in lesioned rats (1.07 ± 0.08) were significantly higher than those in unlesioned control rats (1.00 ± 0.06, $P < 0.05$). On immunohistochemical staining, activated microglia were exclusively observed in the injured right ST but not in the non-injured left ST of the injury rats and the bilateral ST of the non-injured control rats.

Conclusions These results suggest that [11C]PK-11195 PET imaging would be a useful tool for evaluating microglial activation in a rat brain injury model.

Keywords Animal PET · Microglia · [11C]PK-11195 · Peripheral benzodiazepine receptors · Rat

H. Toyama (✉) · G. Kudo · F. Ito · K. Katada
Department of Radiology, Fujita Health University, 1-98
Dengakugakubo, Kutsukake, Toyoake, Aichi 470-1192, Japan
e-mail: htoyama@fujita-hu.ac.jp

K. Hatano · S. Momosaki · T. Kato · H. Yamaguchi · K. Ito
Department of Brain Science and Molecular Imaging, National
Institute for Longevity Sciences, Obu, Japan

H. Suzuki · M. Sawada
Department of Brain Life Science, Research Institute of
Environmental Medicine, Nagoya University, Nagoya, Japan

M. Ichise
Department of Radiology, Columbia University, New York,
NY, USA

Introduction

In the central nervous system (CNS), microglia are major glial components and become activated in response to a wide variety of pathological stimuli such as brain injury and degeneration [1–3]. There is increasing evidence that microglia play an active part in degenerative CNS diseases. In Alzheimer's disease (AD), activated microglia appear to be involved with the plaque formation [2]. In the normal adult CNS, microglia constitute relatively stable cell population [4]. The activated microglial cell

following injury or degeneration undergoes morphological transformation [4]. The transition of microglia from the normal resting state to the activated state is also associated with an increased expression of receptors known as peripheral benzodiazepine receptors (PBRs). Because PBRs are very few in resting microglia, increased PBRs may be used as a marker for detecting activated microglia in vivo, which in turn may be a marker for an active inflammatory disease in the brain [1]. Positron emission tomography (PET) imaging of microglial activation using [^{11}C]PK-11195, a specific PBRs ligand, has been investigated in several neurological conditions such as Parkinson's disease animal model [5], AD [6], and HIV-associated dementia [7] in humans. [^{11}C]PK-11195 with a relatively low affinity for the PBRs is unfortunately unable to show any significant signals from low PBRs densities in the normal brain with inactivated microglia [8–10]. However, the absence of signals in the normal brain does not imply that there are no PBRs in the brain. In contrast, PBRs are widely distributed throughout the normal brain [4]. Here, there is actually no brain tissue devoid of receptors (reference tissue). In this situation with no reference tissue, traditionally a total distribution volume (V) has been used as a PET-measured receptor parameter. However, the estimation of V usually requires invasive arterial blood sampling and tracer metabolite analysis to characterize an input function. In addition, any reference tissue models may have difficulty with very noisy data particularly for pixel time activity curves (TACs) in parametric imaging owing to a poor brain uptake of [^{11}C]PK-11195. In the present study, we evaluated the PBRs binding in a rat brain injury model using [^{11}C]PK-11195 and animal PET with regions of interest (ROIs)-based approach to estimate V. We used an integral from 0 min to 60 min (V_{60}) as an estimate of V and differences in right/left ST V_{60} ratios between lesioned and unlesioned control rats. The PET findings were then compared with qualitative immuno-histochemical findings.

Materials and methods

Preparation of [^{11}C]PK-11195

[^{11}C]PK-11195 was prepared from enantiomerically pure desmethyl precursor following the method reported earlier [11]. [^{11}C]methyl iodide, which was obtained using the conventional LiAlH$_4$ method, was trapped in 0.3 ml of NaOH/DMSO suspension containing (R)-N-desmethyl PK-11195 PLUS (1 mg, ABX, Dresden, Germany). The mixture was then heated at 100°C for 3 min followed by high-performance liquid chromatog-raphy (HPLC) purification. The fraction corresponding to [^{11}C]PK-11195 was collected and evaporated to dryness in vacuo. The residue was dissolved in 0.25% solution of Tween 80 in physiological saline. The radiochemical yield of the synthesis was 20.3% ± 5.9% (13.1%–30.8%) with decay correction. Analytical HPLC revealed that radiochemical purity of the product exceeded 98% and the specific radioactivity was 68.2 ± 18.1 GBq/μmol (39.5–88 GBq/μmol) at the end of the synthesis.

Operating procedure

All the procedures were conducted in accordance with the Guidelines for the National Institutes of Health and Animal Experimentation of the Fujita Health University, School of Medicine.

A novel ethanol injury model established by Takeuchi et al. [12] inducing microglial increment was made as follows.

Wild-type male Fisher rats (8–9 weeks, Charles River, Japan) were used in this study. Rats were anesthetized by intraperitoneal injection (50 mg/kg) of pentobarbital and placed on a stereotaxic frame (Narishige, Japan). The scalp was cleaned with an iodine solution and incised on the midline, and the hole was made in the skull at the appropriate stereotaxic location using a micro-drill. Unilateral intrastriatal administration (right side) of 8 μl of ethanol was performed using a 10-μl Hamilton syringe [12]. Ethanol was infused into the right ST at a rate of approximately 1 μl/min. The stereotaxic coordinates of the target site was anterior = 0.4 mm, lateral = 3 mm, and ventral = 4.5 mm from the Bregma, according to the atlas of Paxinos and Watson [13]. After the injection, the needle was placed for additional 10 min, and then slowly withdrawn.

MRI study

Two days after the surgery (day 3), MRI was performed using a clinical MR equipment, SIGNA INFINITY EXCITE system (1.5 T, GE Healthcare, Milwaukee, WI, USA), and wrist coil (Q-WRIST, GE Healthcare) to detect the extent of injury on the rat right striatum (ST) without killing prior to the PET studies. We have developed feasible techniques that can obtain high-resolution rat brain images to identify the ST stereotactically in a consistent and repetitive manner with neither high magnetic field MR imaging system nor stereotaxic device dedicated for rodent. The positioning principle of our technique which consists of three-plane localization method based on the MR images utilizes the localization principle of the widely used rat brain atlas by Paxinos and Watson [13].

Briefly, rat skull surface was exposed and Bregma was identified. Copper sulfate solution in 10 mm hematocrit glass tube sealed bilateral ends for MR marker and was secured with tissue adhesive right above the Bregma under chloral hydrate (300 mg/kg) i.p. injection anesthesia. Rat head, body, arms, and legs were then fixed using surgical tape with prone position on acryl plate. The rat head on the acryl plate was inserted into the suitable size wrist coil, which was applicable for small radio frequency head coil on the MRI scanner bed.

First three planes (axial, coronal, and sagittal sections) were taken simultaneously (TR/TE = 55.3/1.8 FOV = 12 × 12 cm) for 44 s; then accurate sagittal planes were acquired on the basis of these three planes correcting the tilt on the horizontal plane (TR/TE = 300/9.2 FOV = 12 × 12 cm) for 69 s. Bilateral external auditory meatus, which determine the interaural line, incisor bar, and Bregma marker were identified on these sagittal planes. Seven T2-weighted coronal images (TR/TE = 2000/102 FOV = 10 × 5 cm, 17 echo train length) for 3 min and 48 s were then taken rectangular to the plane between interaural line and incisor bar. A third slice image from the front was set on the Bregma marker which corresponds to the ST plane (Fig. 1). The slice thickness was 3 mm. Image matrix was 320 × 256.

We performed five ethanol-injured rats in one experiment day and scanned using MRI. We performed following PET scanning only for rats which showed high-intensity area around the ethanol-injected right ST on the T2-weighted images (Fig. 1).

PET study

We used the SHR-2000 animal PET device (Hamamatsu Photonics, Hamamatsu, Japan), which provides a 14-slice image set with a maximal image spatial resolution of 3.5 mm full width at half maximum [14].

The next day (day 4), we performed PET scanning for 17 ethanol-injured rats (159–203 g, 180.2 ± 16.2 g) and 7 non-treated rats (125–240 g, 158.2 ± 46.9 g) for control.

A 24-G indwelling needle (Terumo, Tokyo, Japan) was inserted into the tail vein under light ether anesthesia, and then chloral hydrate (300 mg/kg) was intraperitoneally injected into rats. Under anesthesia the rat head was fixed using an originally designed acrylic head holder by modifying a stereotaxic holder used in physiological experiments (Hamamatsu Photonics) [15] based on the rat brain atlas by Paxinos and Watson [13]. The positioning principle was a three-point fixation, consisted of two earplugs and incisor bar [16]. Correction of photon

Fig. 1 Representative coronal magnetic resonance imaging (MRI) T2-weighted images (*arrow* in *left top row* showing ethanol injury lesion), summed images (0–60 min) of ^{11}C-PK-11195 positron emission tomography (PET) in ethanol-injured rat (*top row right*) and normal control rat (*bottom row right*) and ^{11}C-raclopride PET (*bottom row left*) with regions of interest on bilateral striatum

Right striatum ethanol injury rat
MRI   ^{11}C-PK-11195 PET

Lt   Rt

Normal control rat
[11]C-raclopride PET   ^{11}C-PK-11195 PET
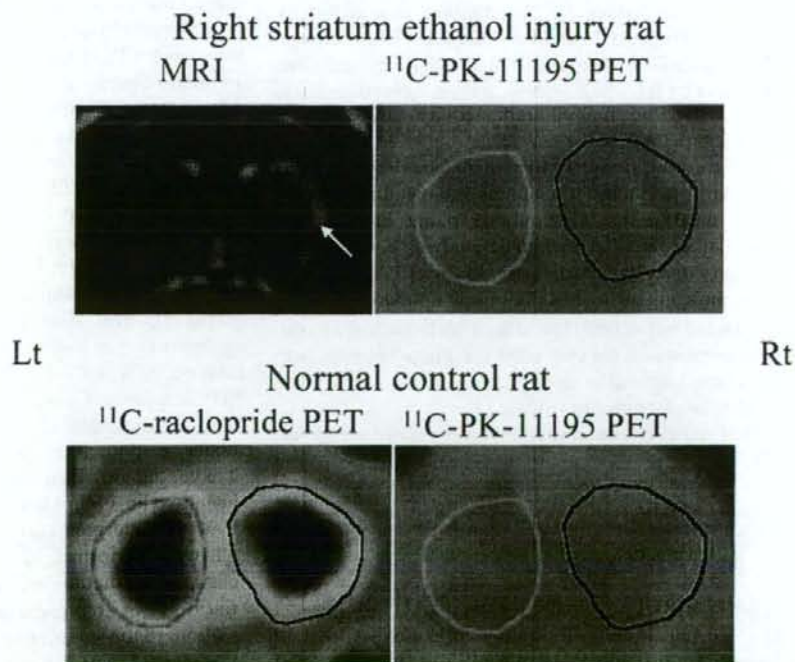
attenuation was carried out with transmission data obtained by rotating the ^{68}Ge/^{68}Ga rod source for 15 min.

Dynamic PET scans (24 frames; frames 8×30 s, 6×60 s, 10×300 s) were acquired for 60 min under continuous infusion of chloral hydrate (100 mg/kg per hour) immediately following a bolus injection of 13–39 MBq of [^{11}C]PK11195 through the tail vein. The body temperature in the anesthetized animals was monitored with a rectal temperature probe and maintained at 31.2–36.5°C with a heating pad. The scanned images of [^{11}C]PK11195 were reconstructed using a Butterworth filter with a cut-off frequency of 144 cycle/cm [17]. The slice thickness was 3 mm. A third slice image from the front was set on the Bregma which corresponds to the ST plane.

PET data analysis

Regions of interest on bilateral ST were placed on the reconstructed images guided by the rat brain atlas by Paxinos and Watson [13], and the reports of Suzuki and Sakiyama [15, 16] (Fig. 1). [^{11}C]raclopride imaging for dopamine D2 receptor was performed to validate the accuracy of ST slice based on our stereotaxic three-point fixation for pilot study and used to delineate ROI on bilateral ST for reference (Fig. 1). ROI values on bilateral ST were divided by the injection dose (kBq) to obtain an image ROIs-derived [^{11}C]PK11195 percentage of the injected dose per gram of tissue (%ID/g), and were multiplied by the whole body weight (in kg) to determine body-weight normalized radioactivity concentration (%ID-kg/g).

For the pilot study, we tried kinetic modeling for four rats using arterial input functions and metabolite analysis to measure the distribution volume and binding potential. However, any kinetic analyses had difficulty with very noisy data particularly for pixel TACs in parametric imaging owing to a poor brain uptake of [^{11}C]PK-11195 relatively arterial blood data (data not shown). In the present study, we evaluated the PBRs binding with ROIs-based approach to estimate an index of [^{11}C]PK-11195 total distribution volume (V).

The total distribution volume can be defined as follows [18]:

$$V = \frac{\int_0^\infty \text{ROI}\, dt}{\int_0^\infty \text{Plasma}\, dt}$$

; a ratio of ROI area under the curve (AUC)-to-plasma AUC to time infinity. In the present study, we used an integral from 0 min to 60 min (V_{60}) as an estimate of

V. V_{60} underestimates V (i.e., $V_{60} < V$), because plasma time activity clears more rapidly than does the ROI time activity. We used V_{60} of the ST of injected side normalized by V_{60} of the uninjected side as an outcome measure, which should be increased if [^{11}C]PK-11195 binding is increased because of inflammation on the injected side, assuming that the underestimation of V by the use of V_{60} is similar on both sides. Thus, we calculated V_{60}(right ST)/V_{60}(left ST) = (right ST AUC/plasma AUC)/(left ST AUC/plasma AUC) = right ST AUC/left ST AUC. Therefore, the calculation of this ratio eliminated the need for blood data. We then compared this ratio between lesioned and unlesioned control rats. The level of statistical significance was designated as $P < 0.05$.

Tissue preparation and histochemical staining

On the PET experiment day (day 4) after the scanning, Fisher rats were deeply anesthetized with pentobarbital (25 mg/kg, i.p.) and exsanguinated by transcardial perfusion with isotonic saline solution, and brains were removed after decapitation. The brain was isolated, frozen in liquid nitrogen, and embedded in OCT compound (Tissue-Tek; Sakura Finetek, Tokyo, Japan). Frozen sections (8 µm) were serially cut into four slices using a microtome (Laica, Solms, Germany), then transferred to gelatin-coated slides and air dried. The sections were fixed with 4% paraformaldehyde in PBS at 4°C for 15 min to determine the location of exogenous microglia relative to the ST area. Sections were labeled with FITC-conjugated Griffonia simplifolia isolectin-B4 (IB4-lectin) (GSA-IB4; Sigma, St. Louis, MO, USA), monoclonal antibodies against ED-1 (Rat leukocyte antigen; BMA, Augst, Switzerland) or ED-2 (rat macrophage antigen; BMA). In brief, sections were incubated for 30 min at room temperature in PBS containing 1% bovine serum albumin, 10% normal goat serum, and 0.01% sodium azide, and then labeled with a monoclonal antibody against ED-1 at a dilution of 1:100 or the ED-2 at a dilution of 1:100. The reaction was visualized with FITC-conjugated goat F(ab9)2 anti-mouse IgG (Rockland) at a dilution of 1:200, and then photographed under a fluorescent microscope (BX-50, Olympus, Tokyo, Japan). Each serial section was stained using hematoxylin–eosin (HE).

Visual interpretations of representative slices of the ST were performed. Quantification of immunohistochemical evaluations was not carried out because quantification of representative thin histochemical slice sections (8 µm) may not be equivalent to the thicker slice thickness (3 mm) PET data.
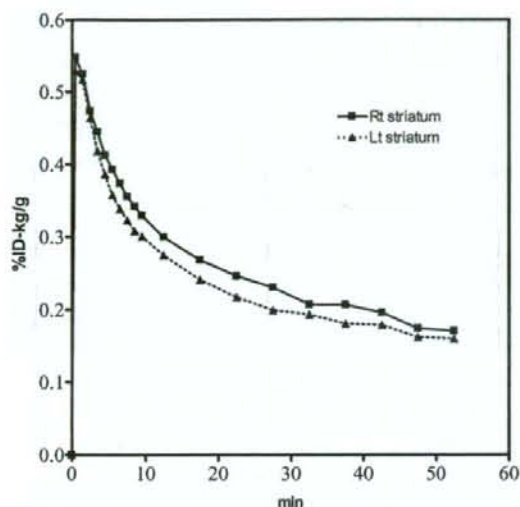
Fig. 2 Averaged time–activity curves of [¹¹C]PK-11195 in lesioned right and unlesioned left striatum in injury rats. For clarity, these figures do not show error bars and are meant to convey only trends
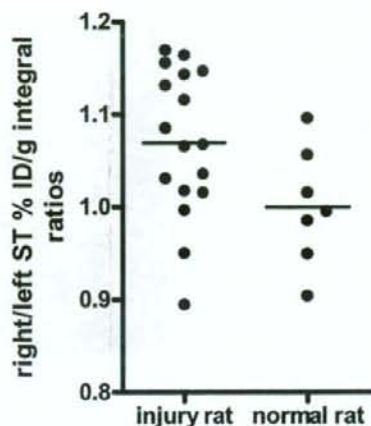

Fig. 3 Comparison of 0–60 min right/left ST %ID/g integral ratios (right/left ST V_{60} ratios) between injury and unlesioned control rats in [¹¹C]PK-11195 brain PET. The ratios in lesioned rats (1.07 ± 0.08) are significantly higher than in unlesioned control rats (1.00 ± 0.06, $P < 0.05$)

Results

PET data analysis

Averaged TACs showed rapid entry and clearance of [¹¹C]PK-11195 in lesioned and unlesioned ST in injury rats (Fig. 2). The highest peaks were 0.56 ± 0.22 %ID-kg/g (3.1 ± 1.14 %ID/g) in lesioned right ST and 0.54 ± 0.23 %ID-kg/g (3.0 ± 1.15 %ID/g) in unlesioned left ST at 0.5 min. There were no significant differences in averaged peak %ID-kg/g values between lesioned and unlesioned ST. In the time course of [¹¹C]PK-11195 activity, [¹¹C]PK-11195 clearance in lesioned right ST was slower than that in unlesioned left ST (Fig. 2).

The 0–60 min right/left ST %ID/g integral ratios (right/left ST V_{60} ratios) in lesioned rats (1.07 ± 0.08) were significantly higher than those in unlesioned control rats (1.00 ± 0.06, $P < 0.05$, Fig. 3).

Histochemical staining of lesioned rats

In HE, a faintly stained, cavernous necrotic area showing coagulation of the tissue and loss of neuronal and glial cells was present around the injected wound in the right ST. On immunohistochemical staining, IB4-lectin and ED-1 positive cells showing activated microglia were exclusively detected in boundary area of the ethanol-injected region in the right ST but neither in the non-

lesioned left ST of the lesioned rats nor in the bilateral ST of the non-lesioned control rats (Fig. 4). To characterize the immunohistochemically stained cells, we double-stained with ED-1 and ED-2. ED-2 that stain macrophage did not stain cell even though activated microglia were detected with ED-1 in lesioned right ST.

Discussion

In this study, [¹¹C]PK-11195, a PET ligand for PBR showed increased binding as expressed in affected/non-affected ST integral ratios (0–60 min, right/left ST V_{60} ratios) between lesioned and unlesioned control rats. These findings are consistent with activated microglia in a rat brain ethanol injury model. The microglia activation was also confirmed by the immunohistochemical staining in the present study.

Price et al. [19] reported that in the ST of sham-lesioned rats [³H]PK-11195 entered brain rapidly, with maximal brain radioactivity occurring within of 2 min of injection and then cleared rapidly. These investigators did not use PET imaging. Rather, they made tracer uptake measurements of dissected brain in a scintillation counter at each time point. They found that the clearance of [³H]PK-11195 in lesioned ST was slower than that in unlesioned ST. In our PET imaging of injury rats, the findings of rapid entry (the highest peaks at 0.5 min) and clearance of [¹¹C]PK-11195 in lesioned and

Fig. 4 Immunohistochemical staining (IB4-lection stain) on the lesioned right and unlesioned left striatum in the same lesioned rat model. Activated microglia are shown in the lesioned right striatum (*arrows*), but not shown in the unlesioned left striatum

Lt striatum   Rt striatum
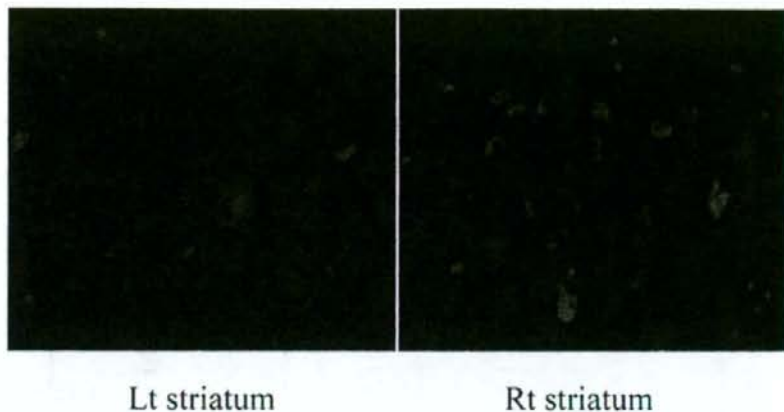
unlesioned ST and slower clearance in lesioned ST than in unlesioned ST are consistent with their ex vivo findings. Cicchetti et al. [5] calculated binding ratios of [^{11}C]PK-11195 between ST and cerebellum with percentage activity of injected dose per pixels in a Parkinson disease rat model induced by unilateral intrastriatal administration of 6-hydroxydopamine using PET. They showed increased [^{11}C]PK-11195 binding by 67% in the lesioned ST and microglial response by immunohistochemistry [5]. In our ethanol injury model, the 0–60 min right/left ST %ID/g integral ratios (right/left ST V_{60} ratios) in lesioned rats were significantly higher than those in unlesioned control rats. However, these differences were only around 7%. In our ethanol injury model, the signal of [^{11}C]PK-11195 in the brain may not be high enough because of low uptake into the brain [8, 9]. Relatively low resolution of our PET scanner might also influence the result of low signal differences. We have obtained rat ST slices on MRI using the three-plane localization method and [^{11}C]PK-11195 PET using stereotaxtic device confirmed by [^{11}C]raclopride uptakes stereotactically for both third slices from the top. Although there are no changes in the ST volume secondary to lesioning, so partial volume should be of the same degree for both sides, accurate MRI and PET fusion techniques would be warranted in the future for much more limited ROI setting on the ethanol injury lesion on the ST using a better resolution PET scanner with less partial volume effect on thinner slice thickness.

Because there is scattering in right/left ST V_{60} ratios in both injury and normal rats, manual ROI setting on bilateral ST might influence the values. Recently, our experiment has shown that increased [^{11}C]PK-11195 binding might be closely related to toxic conversion of activated micloglia not just only the number of activated

microglia (data not shown). Inflammatory cytokines for markers of toxic conversion might be significant to subdivide the widely varied right/left ST V_{60} ratios in injury rats.

An initial PET study using [^{11}C]PK-11195 evaluated with average counts per voxel normalized to cerebellum also showed no detectable alteration in patients with mild to moderate AD probably because of low specific to non-specific binding ratios in mild to moderate AD [10]. However, the Hammersmith hospital group has developed cluster analysis to calculate binding potential for the extraction of voxels with normal ligand kinetics to serve as the reference input function which voxels in the raw dynamic data are segmented into 10 clusters distinguished by the shape of their TACs [1, 20]. They showed significantly increased regional [^{11}C]PK-11195 binding in patients with mild to moderate AD and minimal cognitive impairment [6]. Their cluster analysis might be useful to detect faint signal of [^{11}C]PK-11195 specific binding. Reference tissue models for the analysis of [^{11}C]PK-11195 have also been reported recently [21, 22]. However, they pointed a limitation of this study for using the cerebellum as a reference tissue because increased specific binding in these structures cannot be excluded [21, 22]. In this rat experiment with small brain and limited number of voxels involved, rather than cluster analysis or reference tissue models, we sought to estimate a more direct measure of PBRs receptor binding by an ROIs-based approach to estimate distribution volume. Strictly speaking, infinity scanning time (practically impossible) should be applied to estimate distribution volume with our ROIs-based approach. In the present study, V_{60} was used as an index of V. V_{60} unlike V is affected to some extent by blood flow. In addition, V_{60} which is calculated as ROI AUC includes the activity

in the brain vascular compartment. Therefore, the increased V_{60} ratio could be partly explained by the possibility that blood flow is increased on the lesioned side. However, there were no significant differences in averaged peak %ID-kg/g values between lesioned and unlesioned ST. The lesioned side may have increased flow, and washout is then expected to be faster. However, the lesioned side shows a similar washout rate to the unlesioned side (Fig. 2). Therefore, the difference in TACs in Fig. 2 is consistent with higher binding in the lesioned side.

Takeuchi et al. [12] have established a novel injury model in the CNS by a stereotaxic injection of ethanol into rat ST to induce necrosis. They first demonstrate that microglial inducible nitric oxide synthase (iNOS) mRNA was induced in vivo after the injury and microglial iNOS is considered to play a pivotal role in eliminating damaged neurons by apoptosis, thereby protecting neuronal circuits from necrotic damage [12]. Barger and Harmon [23] showed that microglia in vitro activated by Alzheimer's amyloid precursor protein release NO via iNOS induction. Thus, microglia in vivo may reveal neurotoxic effects via producing NO under certain conditions [12]. Some advantages of our injury model are that the stereotaxic operation seems to produce less damage to other places in the brain than other models such as needle-penetrating wounds, and suction on the brain surface [24, 25]; and necrotic damage seems to be free from hemorrhage and infection owing to the coagulating and sterilizing effects of ethanol [12]. We performed PET scanning for only those rats that showed a high intensity area around the ethanol injected right ST on the T2-weighted images for the ideal injury model. However, in double staining with ED-1 and ED-2, positive cells showing activated microglia were detected in the injured right ST with ED-1, but ED-2 that stains macrophage did not stain cell. Increased PBRs binding in our model would represent the activated microglia, and not owing to macrophages that have crossed through blood–brain barrier leakage. We have not performed the quantification for the immunohistochemical evaluation as mentioned in "Materials and methods". We will compare between the number of activated microglia equivalent to PET slices and PBR binding on PET in the future work.

Recently, novel PET PBRs ligands such as [^{11}C]DAA 1106 [26, 27] and [^{11}C]PBR28 [28, 29] which have higher specific binding compared with [^{11}C]PK-11195 have been developed. Higher specific binding ligands to PBR would be expected to have higher sensitivity of the detection of over expression of PBRs binding sites in the activated microglial cells following injury or degeneration in the brain using in vivo PET imaging.

Conclusions

In this study, [^{11}C]PK-11195, a PET PBR ligand showed increased binding as expressed in affected/non-affected ST integral ratios (0–60 min) between lesioned and control rats consistent with activated microglia in a rat brain ethanol injury model.

These results suggest that [^{11}C]PK-11195 PET imaging and our ROIs-based approach to estimate distribution volume might be a useful tool to evaluate in vivo microglial activation in a rat brain injury model.

References

1. Banati RB. Visualizing microglial activation in vivo. Glia 2002;40:206–17.
2. Stoll G, Jander S. The role of microglia and macrophages in the pathophysiology of the CNS. Prog Neurobiol 1999;58: 233–47.
3. Banati RB, Egensperger R, Maassen A, Hager G, Kreutzberg GW, Graeber MB. Mitochondria in activated microglia in vitro. J Neurocytol 2004;33:535–41.
4. Ladeby R, Wirenfeldt M, Garcia-Ovejero D, Fenger C, Dissing-Olesen L, Dalmau I, et al. Microglial cell population dynamics in the injured adult central nervous system. Brain Res Brain Res Rev 2005;48:196–206.
5. Cicchetti F, Brownell AL, Williams K, Chen YI, Livni E, Isacson O. Neuroinflammation of the nigrostriatal pathway during progressive 6-OHDA dopamine degeneration in rats monitored by immunohistochemistry and PET imaging. Eur J Nerurosci 2002;15:991–8.
6. Cagnin A, Brooks DJ, Kennedy AM, Gunn RN, Myers R, Turkheimer FE, et al. In-vivo measurement of activated microglia in dementia. Lancet 2001;358:461–7.
7. Hammoud DA, Endres CJ, Chander AR, Guilarte TR, Wong DF, Sacktor NC, et al. Imaging glial cell activation with [^{11}C]-R-PK 11195 in patients with AIDS. J Neurovirol 2005; 11:346–55.
8. Debruyne JC, Van Laere KJ, Versijpt J, De Vos F, Eng JK, Striickmans K, et al. Semiquantification of the peripheral-type benzodiazepine ligand [^{11}C]PK11195 in normal human brain and application in multiple sclerosis patients. Acta Neurol Belg 2002;102:127–35.
9. Zhang MR, Maeda J, Ogawa M, Noguchi J, Ito T, Yoshida Y, et al. Development of a new radioligand, N-(5-fluoro-2-phenoxyphenyl)-N-(2-[^{18}F]fluoroethyl-5-methoxybenzyl) acetamide, for PET imaging of peripheral benzodiazepine receptor in primate brain. J Med Chem 2004; 47:2228–35.

10. Groom GN, Junck L, Foster NL, Frey KA, Kuhl DE. PET of peripheral benzodiazepine binding sites in the microgliosis of Alzheimer's disease. J Nucl Med 1995;36:2207–10.

11. Shah F, Hume SP, Pike VW, Ashworth S, McDermott J. Synthesis of the enantiomers of [N-methyl-^{11}C]PK 11195 and comparison of their behaviors as radioligands for PK binding sites in rats. Nucl Med Biol 1994;21:573–81.

12. Takeuchi A, Isobe KI, Miyaishi O, Sawada M, Fan ZH, Nakashima I, et al. Microglial NO induces delayed neuronal death following acute injury in the striatum. Eur J Neurosci 1998;10:1613–20.

13. Paxinos G, Watson C. The rat brain in stereotaxic co-ordinates. 4th ed. San Diego: Academic; 1998.

14. Watanabe M, Uchida H, Okada K, Shimizu K, Satoh N, Yoshikawa E, et al. A high resolution PET for animal studies. IEEE Trans Med Imaging 1992;11:577–80.

15. Suzuki M, Hatano K, Sakiyama Y, Kawasumi Y, Kato T, Ito K. Age-related changes of dopamine D_1-like and D_2-like receptor binding in the F344/N rat striatum revealed by positron emission tomography and in vitro receptor autoradiography. Synapse 2001;41:285–93.

16. Sakiyama Y, Hatano K, Tajima T, Kato T, Kawasumi Y, Suzuki M, et al. An atlas-based image registration method for dopamine receptor imaging with PET in rats. Ann Nucl Med 2007;21:455–62.

17. Momosaki S, Hatano K, Kawasumi Y, Kato T, Hosoi R, Kobayashi K, et al. Rat-PET study without anesthesia: anesthetics modify the dopamine D_1 receptor binding in rat brain. Synapse 2004;54:207–13.

18. Lassen NA. Neuroreceptor quantitation in vivo by the steady-state principle using constant infusion or bolus injection of radioactive tracers. J Cereb Blood Flow Metab 1992;12:709–16.

19. Price GW, Ahier RG, Hume SP, Myers R, Manji L, Cremer JE, et al. In vivo binding to peripheral benzodiazepine binding sites in lesioned rat brain: comparison between [^{3}H]PK11195 and [^{18}F]PK14105 as markers for neuronal damage. J Neurochem 1990;55:175–85.

20. Gunn RN, Lammertsma AA, Hume SP, Cunningham VJ. Parametric imaging of ligand–receptor interactions using a reference tissue model and cluster analysis. In: Carson R, Daule M, Witherspoon P, Herscovitch P, editors. Quantitative functional brain imaging with positron emission tomography. San Diego: Academic; 1998; p. 401–6.

21. Kropholler MA, Boellaard R, Schuitemaker A, Folkersma H, van Berckel BNM, Lammertsma A. Evaluation of reference tissue models for the analysis of [^{11}C](R)-PK11195 studies. J Cereb Blood Flow Metab 2006;26:1431–41.

22. Schuitemaker A, van Berckel BNM, Kropholler MA, Veltman DJ, Scheltens P, Jonker C, et al. SPM analysis of parametric (R)-[^{11}C]-PK11195 binding images: plasma input versus reference tissue parametric methods. Neuroimage 2007;35:1473–79.

23. Barger SW, Harmon AD. Microglial activation by Alzheimer amyloid precursor protein and modulation by apolipoprotein E. Nature 1997;388:878–81.

24. Cavanagh JB. The proliferation of astrocytes around a needle wound in the rat brain. J Anat 1970;106:471–87.

25. Finklestein S, Campbell A, Stoll AL, Baldessarini RJ, Stinus L, Paskevitch PA, et al. Changes in cortical and subcortical levels of monoamines and their metabolites following unilateral ventrolateral cortical lesions in the rat. Brain Res 1983;271:279–88.

26. Zhang MR, Kida T, Noguchi J, Furutsuka K, Maeda J, Suhara T, et al. [^{11}C]DAA1106: radiosynthesis and in vivo binding to peripheral benzodiazepine receptors in mouse brain. Nucl Med Biol 2003;30:513–9.

27. Maeda J, Suhara T, Zhang MR, Okauchi T, Yasuno F, Ikoma Y, et al. Novel peripheral benzodiazepine receptor ligand [^{11}C]DAA1106 for PET: an imaging tool for glial cells in the brain. Synapse 2004;52:283–91.

28. Imaizumi M, Kim HJ, Zoghbi SS, Briard E, Hong J, Musachio JL, et al. PET imaging with [^{11}C]PBR28 can localize and quantify upregulated peripheral benzodiazepine receptors associated with cerebral ischemia in rat. Neurosci Lett 2007;411:200–5.

29. Imaizumi M, Briard E, Zoghbi SS, Gourley JP, Hong J, Musachio JL, et al. Kinetic evaluation in nonhuman primates of two new PET ligands for peripheral benzodiazepine receptors in brain. Synapse 2007;61:595–605.

Neurobiology of Disease

Imaging of Peripheral Benzodiazepine Receptor Expression as Biomarkers of Detrimental versus Beneficial Glial Responses in Mouse Models of Alzheimer's and Other CNS Pathologies

Bin Ji,[1] Jun Maeda,[1] Makoto Sawada,[2] Maiko Ono,[1] Takashi Okauchi,[1] Motoki Inaji,[1] Ming-Rong Zhang,[1] Kazutoshi Suzuki,[1] Kiyoshi Ando,[1,3] Matthias Staufenbiel,[4] John Q. Trojanowski,[5] Virginia M. Y. Lee,[5] Makoto Higuchi,[1] and Tetsuya Suhara[1]

[1]Molecular Imaging Center, National Institute of Radiological Sciences, Chiba, Chiba 263-8555, Japan, [2]Department of Brain Function, Research Institute of Environmental Medicine, Nagoya University, Nagoya, Aichi 464-8601, Japan, [3]Nonhuman Primate Laboratory, Central Institute for Experimental Animals, Kawasaki, Kanagawa 216-0001, Japan, [4]Novartis Institutes for Biomedical Research–Basel, CH-4002 Basel, Switzerland, and [5]Center for Neurodegenerative Disease Research, University of Pennsylvania, Philadelphia, Pennsylvania 19104

We demonstrate the significance of peripheral benzodiazepine receptor (PBR) imaging in living mouse models of Alzheimer's disease (AD) as biomarkers and functional signatures of glial activation. By radiochemically and immunohistochemically analyzing murine models of the two pathological hallmarks of AD, we found that AD-like Aβ deposition is concurrent with astrocyte-dominant PBR expression, in striking contrast with nonastroglial PBR upregulation in accumulations of AD-like phosphorylated tau. Because tau-induced massive neuronal loss was distinct from the marginal neurodegeneration associated with Aβ plaques in these models, cellular localization of PBR reflected deleterious and beneficial glial reactions to tau versus Aβ pathologies, respectively. This notion was subsequently examined in models of various non-AD neuropathologies, revealing the following reactive glial dynamics underlying differential PBR upregulation: (1) PBR(−) astrogliosis uncoupled with microgliosis or coupled with PBR(+) microgliosis associated with irreversible neuronal insults; and (2) PBR(+) astrogliosis coupled with PBR(− or ±) microgliosis associated with minimal or reversible neuronal toxicity. Intracranial transplantation of microglia also indicated that nontoxic microglia drives astroglial PBR expression. Moreover, levels of glial cell line-derived neurotrophic factor (GDNF) in astrocytes were correlated with astroglial PBR, except for increased GDNF in PBR(-) astrocytes in the model of AD-like tau pathology, thereby suggesting that PBR upregulation in astrocytes is an indicator of neurotrophic support. Together, PBR expressions in astrocytes and microglia reflect beneficial and deleterious glial reactions, respectively, in diverse neurodegenerative disorders including AD, pointing to new applications of PBR imaging for monitoring the impact of gliosis on the pathogenesis and treatment of AD.

Key words: neurodegenerative disorders; microglia; astrocyte; peripheral benzodiazepine receptor; glial cell line-derived neurotrophic factor; Alzheimer's disease

Introduction

A growing body of neuropathological evidence has demonstrated that concurrent microglial and astroglial activation accompanies neurodegeneration in Alzheimer's disease (AD) (Dickson et al., 1993; McGeer and McGeer, 2003) and other related disorders (Arnold et al., 2000; Nelson et al., 2002; Wojtera et al., 2005; Kim and Joh, 2006). In AD, excessive glial responses to the accumulation of Aβ are thought to augment progressive neuronal injury

(Combs et al., 2000; Qin et al., 2002). Meanwhile, Aβ immunotherapies have been developed based on a mechanistic concept that induction of microglial responses contribute to the elimination of pathological Aβ aggregates (Schenk et al., 1999; Dodel et al., 2003). Thus, there may be a bifunctionality of reactive gliosis (Zilka et al., 2006; Fiala et al., 2007), but this notion remains elusive without the aid of appropriate biological markers reflecting deleterious and/or beneficial modes of glial responses.

Peripheral benzodiazepine receptor (PBR) (also known as translocator protein) was initially known to be expressed in activated microglia (Myers et al., 1991; Stephenson et al., 1995; Banati, 2002), although it has more recently been revealed that reactive astrocytes also exhibit noticeable levels of PBR (Chen et al., 2004; Maeda et al., 2007a; Rojas et al., 2007). Further, radiolabeled imaging agents have permitted sensitive detection of glial PBR when applied to *in vitro* autoradiographic and *in vivo* positron emission tomographic (PET) techniques. For example,

[¹¹C]PK11195 was the first to enable PET measurement of PBR in diverse CNS pathologies (Banati et al., 2000; Pappata et al., 2000; Cagnin et al., 2001; Rojas et al., 2007), but other radiolabeled ligands were developed, such as (N-5-fluoro-2-phenoxyphenyl)-N-(2-hydroxy-5-methoxybenzyl)acetamide (or DAA1106) with ¹¹C and ¹⁸F resulting in the production of [¹¹C]DAA1106 and [¹⁸F]fluoroethyl-DAA1106 ([¹⁸F]FE-DAA1106), respectively, to establish PET tracers suitable for imaging PBR in living brains (Zhang et al., 2003, 2004; Fujimura et al., 2006; Ikoma et al., 2007; Venneti et al., 2007).

Based on these technical progresses, the present study was aimed at elucidating the significance of PBR upregulation in microglia and astrocytes. The analyses were initiated by radiochemically and immunohistochemically examining two distinct models of AD, mutant amyloid precursor protein (APP) and tau transgenic (Tg) mice (Sturchler-Pierrat et al., 1997; Yoshiyama et al., 2007). The tau Tg mice show a progressive and substantial loss of neurons (Yoshiyama et al., 2007), in clear contrast to the APP Tg mice that show only minimal or no neuronal death (Van Dam et al., 2005). Moreover, our PBR imaging has demonstrated that gliosis accelerates tau-induced neurodegeneration (Yoshiyama et al., 2007), which contrasts with the amelioration of Aβ deposition by microglial activation in APP Tg mice (Maeda et al., 2007b). We thus presumed that the cellular profiles of PBR expression in tau and APP Tg mice could distinguish the ameliorative versus deleterious responses of microglia and astrocytes to accumulations of pathological Aβ and tau in AD. We also extended these studies by examining the general mechanism by which PBR is differentially upregulated in microglia and astrocytes using other experimental models of CNS injuries.

Materials and Methods

Reagents and antibodies. The following reagents and all other chemicals were of analytical grade and commercially purchased: methamphetamine (METH), 6-hydroxydopamine (6-OHDA) and kainic acid (KA) from Wako Pure Chemicals; 1-methyl-4-phenyl-1,2,3,6-tetrahydropyridine (MPTP), horseradish peroxidase-conjugated isolectin B4 from *Griffonia simplicifolia* (HRP-ILB4), cuprizone, GBR12909 and PK11195 from Sigma-Aldrich.

We raised a rabbit polyclonal antibody against the C-terminal sequence of PBR using synthetic peptide spanning residues 155–169 of murine PBR (WRDNSGRRGGSRLAE). This antibody (NP155) was affinity-purified and characterized by immunoblotting as well as immunostaining for comparison with commercial anti-PBR antibodies (rabbit polyclonal, R&D Systems; rabbit polyclonal, BioVision; rabbit polyclonal, FL-169, Santa Cruz Biotechnology; goat polyclonal, W-12, Santa Cruz Biotechnology). Other antibodies used in this study are as follows: rabbit polyclonal antibody against ionized calcium binding adapter molecule-1 (Iba-1) (Wako Pure Chemicals), mouse monoclonal antibody against rat CD11b (OX42; AbD Serotec), rat monoclonal antibody against mouse CD11b (M1/70; BMA Biomedicals), rabbit polyclonal (Dako) and rat monoclonal (clone 2.2B10; Zymed/Invitrogen) antibodies against glial fibrillary acidic protein (GFAP), rat monoclonal antibody against myelin basic protein (MBP) (Millipore), rabbit polyclonal antibody against glial cell line-derived neurotrophic factor (GDNF) (Santa Cruz Biotechnology) and rabbit polyclonal antibody against tyrosine hydroxylase (TH) (Millipore).

Western blot analysis. For evaluation of NP155, the microglial clone termed Ra2 was maintained in Eagle's minimum essential medium (M4655; Sigma-Aldrich) supplemented with 10% fetal bovine serum, 5 μg/ml bovine insulin, 0.2% glucose and 1 ng/ml murine granulocyte-macrophage colony-stimulating factor (G0282; Sigma-Aldrich), as described previously (Sawada et al., 1998). For biochemical analyses, the cells (5 × 10⁶) were scraped and homogenized in 50 mM Tris-HCl, pH 7.4, 4°C, containing 0.1% protease inhibitor mixture (5 mM leupeptin, 1 mg pepstatin and 5 mg aprotinin in 1 ml dimethyl sulfoxide) and 0.5 mM

phenylmethylsulfonyl fluoride (PMSF). The suspension was centrifuged at 12,000 rpm (10,000 × g) for 15 min, and the resultant pellet was resuspended in 50 mM Tris-HCl buffer. The protein amounts in the samples were measured according to Lowry's method. For immunocytochemistry, the cells were cultured on cover glasses for 7 d, and washed with PBS, followed by fixation with 4% paraformaldehyde for 20 min.

Hippocampal samples from KA-treated and untreated rats were homogenized in 50 mM Tris-HCl, pH 7.4, 4°C, containing 0.1% protease inhibitor mixture (as in experiment for Ra2 cells) and 0.5 mM PMSF. The suspended homogenates of cultured microglial (Ra2) cells and rat hippocampal tissues, corresponding to 10 and 100 μg protein, respectively, were applied to a 15% SDS polyacrylamide gel. After electrophoresis and transfer of proteins to a polyvinylidene fluoride membrane (Immobilon-P; Millipore), the membrane was immersed in Tris-buffered saline (150 mM NaCl, 10 mM Tris-HCl, pH 8.0) containing 0.05% (v/v) Tween 20 and 3% (w/v) bovine serum albumin (BSA), and then reacted for 1 h with anti-PBR antibodies in TBS containing 0.05% (v/v) Tween 20 and 0.1% (w/v) BSA. The primary antibodies were detected by HRP-conjugated anti-IgG antibodies (GE Healthcare) and enhanced chemiluminescence method (GE Healthcare).

Animal models. The mice studied here were maintained and handled in accordance with the National Research Council's Guide for the Care and Use of Laboratory Animals and our institutional guidelines. Protocols for the present animal experiments were approved by the Animal Ethics Committees of the National Institute of Radiological Sciences and Central Institute for Experimental Animals (CIEA).

APP Tg mice termed APP23, which overexpress the Swedish doubly mutant APP751 under the control of a neuron-specific Thy-1 promoter element, were developed as described in detail previously (Sturchler-Pierrat et al., 1997), and were maintained on a C57BL/6J background. Tau Tg mice dubbed PS19 were generated by using a cDNA coding a tau isoform containing 1 N-terminal and 1 C-terminal alternatively spliced exons and the P301S *MAPT* mutation discovered in frontotemporal dementia with parkinsonism linked to chromosome 17 in combination with a murine prion protein promoter (Yoshiyama et al., 2007). The strain was maintained on a B6C3H background. Littermates were used as controls.

Models of KA-induced excitotoxicity were generated by intraperitoneally administering KA (12 mg/kg) to male Sprague Dawley rats (Japan SLC, Hamamatsu) at 8 weeks of age. All rats analyzed here presented visible cramps within 1 h of KA injection. At 1 week after KA challenge, the animals were deeply anesthetized with sodium pentobarbital and transcardially perfused with PBS, and brain tissues were removed. One hemisphere was immediately frozen with dry ice and stored at −80°C pending assays. The other hemisphere was fixed with 4% paraformaldehyde in phosphate buffer.

Selective injury to the nigrostriatal dopaminergic system was caused in mice, rats and marmosets by the use of METH, 6-OHDA and MPTP, respectively. Male in-house C57BL/6J mice (Kito et al., 2003) aged 8 weeks were subcutaneously injected with METH (5 mg/kg) 4 times, 2 h apart, and brain tissues of these mice were obtained at 2 and 7 d after treatment, as in the protocol for KA-injected rats. Lesioning of rat brains was performed as described previously (Inaji et al., 2005). Briefly, male Sprague Dawley rats (Japan SLC) at 8 weeks of age were anesthetized with intraperitoneally administered sodium pentobarbital (60 mg/kg) and placed in a stereotactic frame (Narishige). Four microliters of 2 μg/μl 6-OHDA, freshly dissolved in physiological saline containing 0.1% ascorbic acid, was subsequently injected into the right medial forebrain bundle (stereotactic coordinates: anteroposterior, 4.2 mm from the bregma; mediolateral, 1.8 mm from the midline; and dorsoventral, 7.8 mm below the dura mater) of each rat at a rate of 1.0 μl/min. The animals were lethally anesthetized with sodium pentobarbital at 1 week after treatment, and brain samples were prepared as in the protocol for KA-injected rats. The MPTP challenge was performed using 10 male and 10 female common marmosets (*Callithrix jacchus*), either in-house bred at CIEA or obtained from CLEA Japan, as in our previous study (Ando et al., 2008). These animals, initially aged 3.8 ± 2.5 years and weighing 316.3 ± 39.6 g, were divided into 2 experimental groups (n = 5 per group) matched for sex, body weight and age. The treatment group consisted

of marmosets receiving 3 doses of subcutaneous MPTP administration (2 mg/kg), 24 h apart, and they were killed by deep anesthetization with sodium pentobarbital at 2 weeks. Their brains were immediately extirpated, frozen with dry ice, and stored at $-80°C$ pending assays. Brains of marmosets in the untreated group were also collected for use as controls.

We also generated a mouse model of massive demyelination by continuously feeding male in-house bred C57BL/6J mice aged 8 weeks with a powdered diet containing 0.2% (w/w) cuprizone, as described previously (Chen et al., 2004). Brain tissues were obtained from these animals at 4 weeks of treatment, as in the protocol for KA-injected rats.

Microglial cell cultures and transplantation. Collected Ra2 cells were labeled with fluorescent dye, PKH26 (MINI26; Sigma-Aldrich), as described previously (Imai et al., 2007), and the final cellular concentration was adjusted to 100,000 cells/μl medium. Male C57BL/6J mice were anesthetized with 1.5% (v/v) isoflurane and were placed in a stereotactic frame (Narishige). Using a 10 μl Hamilton syringe, 2 μl of cell suspension and medium alone were injected into the right and left hippocampi, respectively (stereotactic coordinates: anteroposterior, -2.8 mm; mediolateral, 2.0 mm; dorsoventral 2.0 mm from the bregma), over 4 min. The needle was left in place for 2 min before being withdrawn. These mice were killed 1 week after the procedure, and brain sections were prepared as in the protocol for KA-injected rats.

Immunocytochemical, immunohistochemical and histochemical analyses. For immunohistochemical assays, the entire brains of animals fixed with 4% paraformaldehyde were cryoprotected using 30% sucrose in phosphate buffer, and 10- or 20-μm-thick frozen sections 40 μm apart were generated in a cryostat (HM560; Carl Zeiss). Alternatively, frozen brain tissues were sliced into 20 μm sections for autoradiographic analysis of dopamine transporter. The brain sections were immunostained based on a standard protocol using either fluorophore-conjugated secondary antibodies (Invitrogen) or a commercial kit for avidin-biotin-diaminobenzidine staining (ABC Staining Systems; Santa Cruz Biotechnology). The sections used for PBR staining were beforehand autoclaved in citric buffer for antigen recovery. Similarly, immunofluorescence staining of Ra2 cells on a cover glass was performed.

Aβ plaques in APP23 mice were visualized by using 0.01% (E,E)-1-fluoro-2,5-bis(3-hydroxycarbonyl-4-hydroxy)styrylbenzene (FSB; Dojindo Laboratories), a fluorescent dye for amyloid fibrils (Maeda et al., 2007b).

Microglial cells in the brain were also histochemically visualized by isolectin labeling. Brain sections were reacted with HRP-ILB4 (10 mg/ml) overnight at 4°C and excess reagent was eliminated by 3 washes in PBS (5 min each). The signals were developed by 3,3′-diaminobenzidine (DAB).

Quantitative analyses were performed using at least 5 slices covering each region of interest (ROI). All stained sections were examined by a confocal laser scanning microscope (FV1000; Olympus) or an all-in-one microscope/digital camera (BZ-9000; Keyence), and photomicrographs captured at 10× (FV1000) or 20× (BZ-9000) were semiautomatically tiled and merged into a large high-resolution image containing the whole ROI. Signal intensities were initially measured for the whole ROI, followed by determination of the overall maximum intensity. A cutoff threshold of the intensity was then assigned for each section as [(background intensity) + (5% of overall maximum intensity)] with additional manual tuning. Areas showing signal intensities above the threshold were calculated for quantification of GFAP-positive astrocytes, and were expressed as ratios against the total area of the ROI. Similarly, areas were estimated for other sections stained with antibodies against PBR, MBP and GDNF. For quantification of Iba-1-immunoreactive microglia, cells containing a hematoxylinophilic nucleus and cytoplasmic Iba-1 signals above the cutoff threshold were counted and expressed as the number per unit area (mm^2). Finally, images for which the quantitative value was close to the group average were selected as representative illustrations in the figures. All these analyses were performed with MetaMorph 6.1 (Universal Imaging) and Photoshop 7.0 (Adobe Systems) software.

Radiosynthesis and autoradiography. Synthesis of ^{11}C-labeled N-(3-iodoprop-2E-enyl)-2β-carbomethoxy-3β-(4-methylphenyl)nortropane ($[^{11}C]$PE2I), a PET ligand for dopamine transporter, was conducted by

O-methylation of its free acid precursor with $[^{11}C]$methyl triflate according to previously described methods (Halldin et al., 2003). The radiochemical purity of the resultant compound was >99%, and the specific radioactivity was 219.2 ± 38.8 GBq/μmol at the end of synthesis.

$[^{18}F]$FE-DAA1106 was radiosynthesized using its desmethyl precursor, DAA1123 (generously provided by Taisho Pharmaceutical), based on a previously described protocol (Zhang et al., 2003, 2004). The radiochemical purity of the end product exceeded 95%, and the specific radioactivity was 120 ± 20.5 GBq/μmol at the end of synthesis. $[^{3}H]$DAA1106 was synthesized by O-methylation of DAA1123 with $[^{3}H]$methyliodide (specific radioactivity, 3.15 TBq/mmol; GE Healthcare). The reaction product was purified as described previously (Maeda et al., 2007a; Yoshiyama et al., 2007).

In vitro autoradiography of dopamine transporters was performed using unfixed frozen brain sections and $[^{11}C]$PE2I, in accordance with the established procedure (Inaji et al., 2005). The sections were preincubated in 50 mm Tris-HCl buffer, pH 7.4, for 30 min at room temperature, followed by reaction with $[^{11}C]$PE2I (18.5 MBq/L, ~20 pm) in 50 mm Tris-HCl buffer, pH 7.4, for 60 min at 25°C. Nonspecific binding of the radioligand was determined by adding a nonradioactive ligand, GBR12909 (10 μm), to the reaction. The samples were then rinsed twice with ice-cold Tris-HCl buffer for 2 min, dipped into ice-cold water for 10 s, warmly blow-dried and contacted to an imaging plate (BAS-MS2025; Fuji Film) for 1 h. Radiolabeling was detected by scanning the imaging plate by means of the BAS5000 system (Fuji Film). Autoradiographic assay for PBR was conducted using paraformaldehyde-fixed frozen sections. The fixation did not affect the binding of this PBR ligand in our preliminary experiments (data not shown). The samples were incubated with $[^{18}F]$FE-DAA1106 (18.5 MBq/L, ~0.35 nm) or $[^{3}H]$DAA1106 (2.4 MBq/L, ~0.5 nm) in 50 mm Tris-HCl. Nonspecific binding of the radioligand was estimated by adding nonradioactive PK11195 (10 μm) to the reaction. The rest of the protocol was as described above. The samples used for $[^{3}H]$DAA1106 autoradiography were then coated with warm photographic emulsion (EM-1; GE Healthcare) and exposed, as described in detail previously (Maeda et al., 2007a). The developed emulsion autoradiograms were examined with a microscope (AX-80; Olympus).

Small animal PET imaging. PET scans were performed using a micro-PET Focus 220 animal scanner (Siemens Medical Solutions) as described previously (Maeda et al., 2007b). Control and cuprizone-administered mice were anesthetized with 1.5% (v/v) isoflurane, and a 30-G needle connected to a 1 ml polypropylene syringe via a length of polyethylene tubing was inserted into the tail vein. After transmission scans for attenuation correction using ^{68}Ge-^{68}Ga point source, emission scans were acquired for 60 min in a 3D list mode with an energy window of 350–750 keV, and intravenous injection of $[^{18}F]$FE-DAA1106 (13.26 ± 14.27 MBq) was performed immediately. Summation images from 0 to 60 min after $[^{18}F]$FE-DAA1106 injection were reconstructed with maximum a posteriori reconstruction, and dynamic images were reconstructed with filtered back-projection using a 0.5 mm Hanning filter. Volumes of interest (VOIs) were placed on striatal areas including the corpus callosum using PMOD image analysis software (PMOD Group) with reference to the MRI template. Tracer uptake in each VOI was estimated as percentage of injected dose per tissue volume (%ID/ml).

Statistical analysis. Statistical analyses for group comparisons were performed by Student's t test or ANOVA followed by Bonferroni's *post hoc* test. Difference between groups was considered significant when the p value was <0.05.

Results

Distinct cellular localizations of PBR in models of Aβ and tau pathologies

Application of $[^{18}F]$FE-DAA1106 to *in vitro* autoradiographic imaging of brain slices generated from 20-month-old APP23 mice illustrated intense PBR accumulation primarily in the hippocampus and entorhinal cortex (Fig. 1A), and subsequent immunostaining of the same sections revealed excellent agreement between PBR radiolabeling and Aβ-positive plaque lesions (Fig. 1B,C). PBR upregulation associated with Aβ deposition was also demonstrated at a higher resolution by microautoradiography using $[^{3}H]$DAA1106 (Fig. 1D)
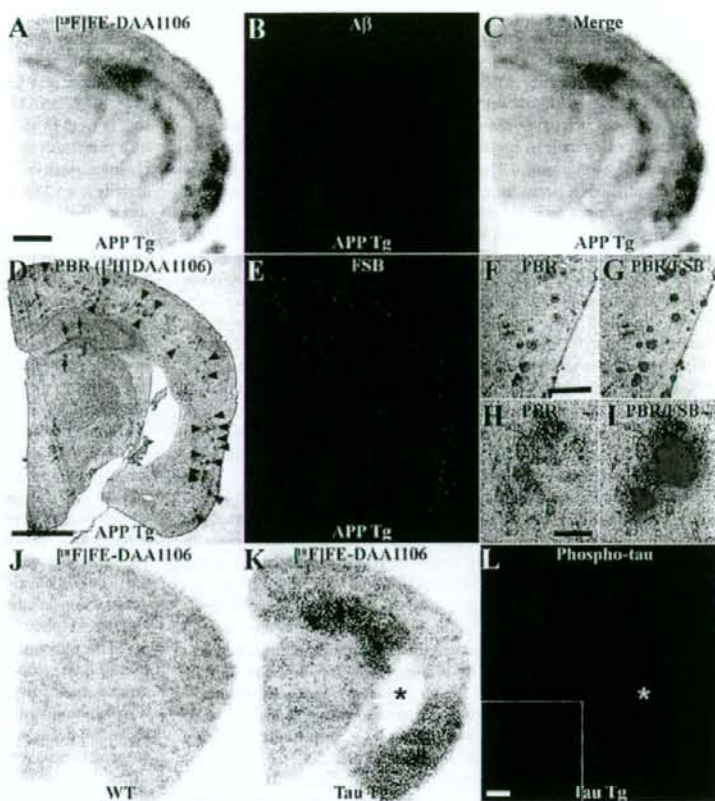
followed by fluorescence staining with FSB (Fig. 1E). High-power photomicrographs for PBR and FSB indicated that the majority of PBR clusters appeared in an annular or semiannular shape outlining the Aβ deposits (Fig. 1F–I). Relative to age-matched WT controls (Fig. 1J), PBR was also markedly upregulated in the hippocampus and entorhinal cortex of 9-month-old PS19 Tg mice (Fig. 1K) in close spatial association with the accumulation of pathologically phosphorylated tau (Fig. 1L). Despite the similarity of regional PBR distributions in the two Tg mouse models, however, the diffuse radiolabeling in PS19 mice concurrent with pronounced hippocampal and entorhinal atrophy and ventricular dilatation contrasted sharply with the patchy and heterogeneous radiographic pattern in the APP23 Tg mice, wherein there was no overt neuronal loss.

Glial subpopulations expressing PBR in these animals were further identified with the aid of NP155, our newly developed anti-PBR antibody, which was shown to detect rodent PBR with a sensitivity and specificity superior to that of the commercially available antibodies (supplemental information; supplemental Fig. 1, available at www.jneurosci.org as supplemental material). Double immunofluorescence staining of GFAP and PBR clearly indicated predominant localization of PBR signals to astrocytes in the vicinity of Aβ plaques in APP23 mice (Fig. 2A–C). Although Iba-1 immunostaining clearly captured the accumulation of activated microglia encompassing amyloid plaques in these mice (Fig. 2D), PBR signals were barely detectable in microglia based on double labeling with NP155 and anti-CD11b antibody M1/70 (Fig. 2D, inset). In striking contrast to the glial response to this Aβ pathology, buildup of phospho-tau in the PS19 mice was accompanied by a pronounced nonastroglial PBR expression because PBR was undetectable in most GFAP-labeled as-

Figure 1. *A–C,* Glial response to plaque deposition as demonstrated by autoradiography for PBR with [18F]FE-DAA1106 in a brain section of a 20-month-old APP23 mouse (*A*) followed by Aβ immunolabeling (*B*; merged image is shown in *C*). *D–I,* Pathology in a 20-month-old APP23 mouse detected by emulsion microautoradiography of [3H]DAA1106 (*D, F, H*) and FSB (*E*), resulting in double labeling of PBR and plaque amyloid (*G, I*). Photomicrographs are displayed at low (*D, E*), middle (*F, G*) and high (*H, I*) magnifications. Correspondence between radiolabeled and fluorolabeled lesions in the hippocampus and neocortex is indicated by arrows and arrowheads, respectively. *J–L,* Brain sections of 9-month-old WT (*J*) and PS19 (*K, L*) mice radiolabeled with [18F]FE-DAA1106 (*J, K*) and immunostained with antibody against phosphorylated tau (*L*). PS19 mouse exhibited PBR positivity and phospho-tau accumulation in the hippocampus and entorhinal cortex, concurrent with marked atrophy of these structures and ventricular dilatation (asterisks in *K, L*). High-power view of hippocampal CA1 sector is shown in inset of *L.* Scale bars: (*A–E, J–L*) 1 mm, (*F, G*) 500 μm, (*H, I*) 100 μm, (inset in *L*) 50 μm.

trocytes (Fig. 2E–G). Meanwhile, numerous amoeboid-shaped Iba-1-immunoreactive microglia were present in the corresponding region (Fig. 2H), and double immunofluorescence staining with NP155 and M1/70 demonstrated that a significant subset of CD11b-positive microglia expressed PBR at a detectable level (Fig. 2H, inset) activated microglia are the primary source of PBR signals in PS19 mice showing tau pathology. Unlike these differential profiles of PBR expression triggered by Aβ and tau lesions, GDNF was upregulated in astrocytes of both models of AD-like plaque and tangle pathology, but GDNF upregulation was insufficient to protect neurons from tau-mediated neurotoxicity in the PS19 mice (Fig. 2I–L).

Astrogliosis without prominent PBR upregulation accompanied by PBR-positive microgliosis in response to excitotoxic insults

We then analyzed diverse experimental models of non-AD neuropathologies to assess PBR expression in glial subtypes after diverse neuronal injuries. As observed in the characterization of NP155 (supplemental Fig. 1, available at www.jneurosci.org as

supplemental material), marked upregulation of PBR was detected in the midbrain as well as hippocampal/entorhinal areas of KA-treated rats. The midbrain regions of these animals were studied further, because different groups of myelinated and unmyelinated neurons in this anatomical structure are present in a well compartmentalized configuration (Fig. 3A, B). Accumulation of Iba-1-immunoreactive microglia was primarily confined to the necrotic core in the substantia nigra pars reticulata and was encircled by GFAP-positive astrocytes, with only a small spatial overlap between distributions of these two glial subpopulations (Fig. 3C–E). Detailed analysis of this lesion by double immunofluorescence staining with NP155 and anti-GFAP antibody revealed that the majority of astrocytes encompassing the microglia-enriched inflammatory epicenter were PBR-negative (Fig. 3F–J). Meanwhile, prominent PBR expression by activated microglia was demonstrated by double immunohistochemical staining with OX42 and NP155 (Fig. 3F–H, K–M, arrowheads). Double labeling also indicated that activated microglia were con-
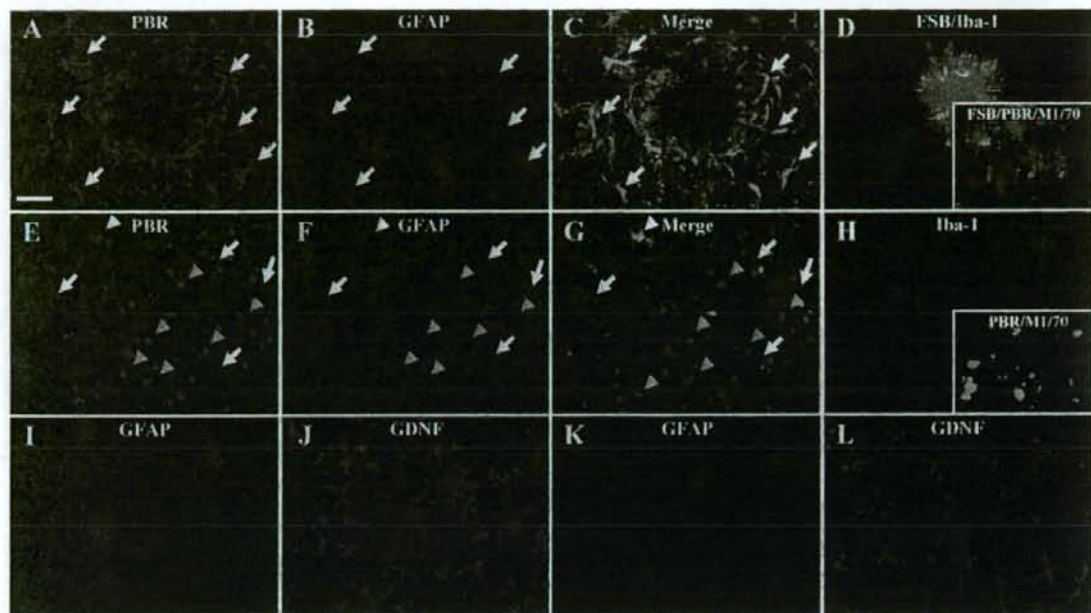
Figure 2. A–D, Glial activation and PBR expression encompassing amyloid plaque in a 20-month-old APP23 mouse. PBR signals (A) were predominantly detected in activated astrocytes (B; 2-channel image in C), although prominent microgliosis (Iba-1; red in D) encircling FSB-positive plaques (blue in D) was observed. Triple staining with FSB (blue in inset of D), NP155 (green in inset of D) and anti-mouse CD11b antibody (M1/70; red in inset of D) also indicated that the majority of plaque-associated microglia did not exhibit intense PBR signals. E–G, Nonastroglial PBR abundantly found in the hippocampus of a 9-month-old PS19 mouse. Double immunostaining for PBR (E) and GFAP (F) indicated that the majority of astrocytes did not express PBR at a detectable level (arrows), and colocalization of PBR and GFAP was observed only in a small subset of PBR-positive astrocytes (white arrowhead; 2-channel image in G), and intense dot-shaped PBR signals (yellow arrowheads) were localized to nonastroglial compartments. H, The same region immunostained for Iba-1, showing numerous microglia with amoeboid shapes distinct from the ramified morphology of resident cells. Double staining with NP155 (green in inset of H) and M1/70 (red in inset of H) revealed that a subset of CD11b-immunoreactive microglia expressed manifest PBRs. I–L, High-level expression of GDNF (J, L) in nearly all GFAP-immunoreactive astrocytes (I, K) reacting to plaque deposition in APP23 mice (I, J) and tau-induced neurotoxicity in PS19 mice (K, L). Scale bars: (A–L) 20 μm, (inset in H) 40 μm.

centrated at the site of prominent demyelination (supplemental Fig. 2 A, D, available at www.jneurosci.org as supplemental material) associated with astrogliosis in the perimeter surrounding this pathology (supplemental Fig. 2 B, E, available at www.jneurosci.org as supplemental material). Interestingly, the loss of TH-positive, unmyelinated dopamine neurons in the substantia nigra pars compacta (supplemental Fig. 2 C, F, available at www.jneurosci.org as supplemental material) was accompanied by astrogliosis (supplemental Fig. 2 E, available at www.jneurosci.org as supplemental material) minimally immunoreactive for PBR but not by any associated microgliosis (supplemental Fig. 2 D, available at www.jneurosci.org as supplemental material). Hence, the excitotoxicity-induced loss of myelinated neurons was tightly linked to PBR-positive microgliosis, whereas damage to unmyelinated neurons did not overtly stimulate microglial activity, both neurotoxic conditions being coexistent with astrogliosis lacking intensified PBR expression.

PBR-negative astrogliosis is uncoupled from prominent microgliosis in injuries of nigrostriatal dopaminergic terminals

To determine if gliosis in response to disruption of the nigrostriatal dopaminergic system is characterized by accumulation of PBR-negative astrocytes and lack of pronounced microglial activation, we examined striatal pathologies in rodent models of neurochemical toxicities. The recruitment of PBR-negative astrocytes after the loss of dopaminergic terminals in the stri-

atum was demonstrated in animals showing selective damage of dopamine neurons. Mice undergoing repeated administrations of METH exhibited progressive loss of striatal dopaminergic terminals up to 7 d after the initiation of treatment, as assessed by autoradiography of dopamine transporter using [¹¹C]PE2I (Fig. 4 A). Meanwhile, elevation of striatal PBR levels was minimal and insignificant according to autoradiographic assay with [¹⁸F]FE-DAA1106 (Fig. 4 B). Histological examinations revealed the activity profiles of glial subtypes, indicating prominent GFAP-positive astrogliosis (supplemental Fig. 3 A, B, G, available at www.jneurosci.org as supplemental material) with very modest microglial alterations (supplemental Fig. 3 C–F, H, available at www.jneurosci.org as supplemental material). Despite marked increase of GFAP immunoreactivity, PBR upregulation was not visible in the striatal astrocytes throughout the observation period (Fig. 4 C–H). We also immunohistochemically analyzed gliotic changes in the striatum of 6-OHDA-injected rats, which developed profound degeneration of the nigrostriatal dopaminergic system (Inaji et al., 2005). As seen in the METH challenge, GFAP signals in the lesioned striatum were substantially increased relative to the contralateral control (supplemental Fig. 3 I–K, available at www.jneurosci.org as supplemental material) with the absence of overt Iba-1-positive microgliosis (supplemental Fig. 3 L–N, available at www.jneurosci.org as supplemental material). This astrogliotic reaction did not coincide with either immunohistochemically (Fig. 4 I–L) or autoradiographi-
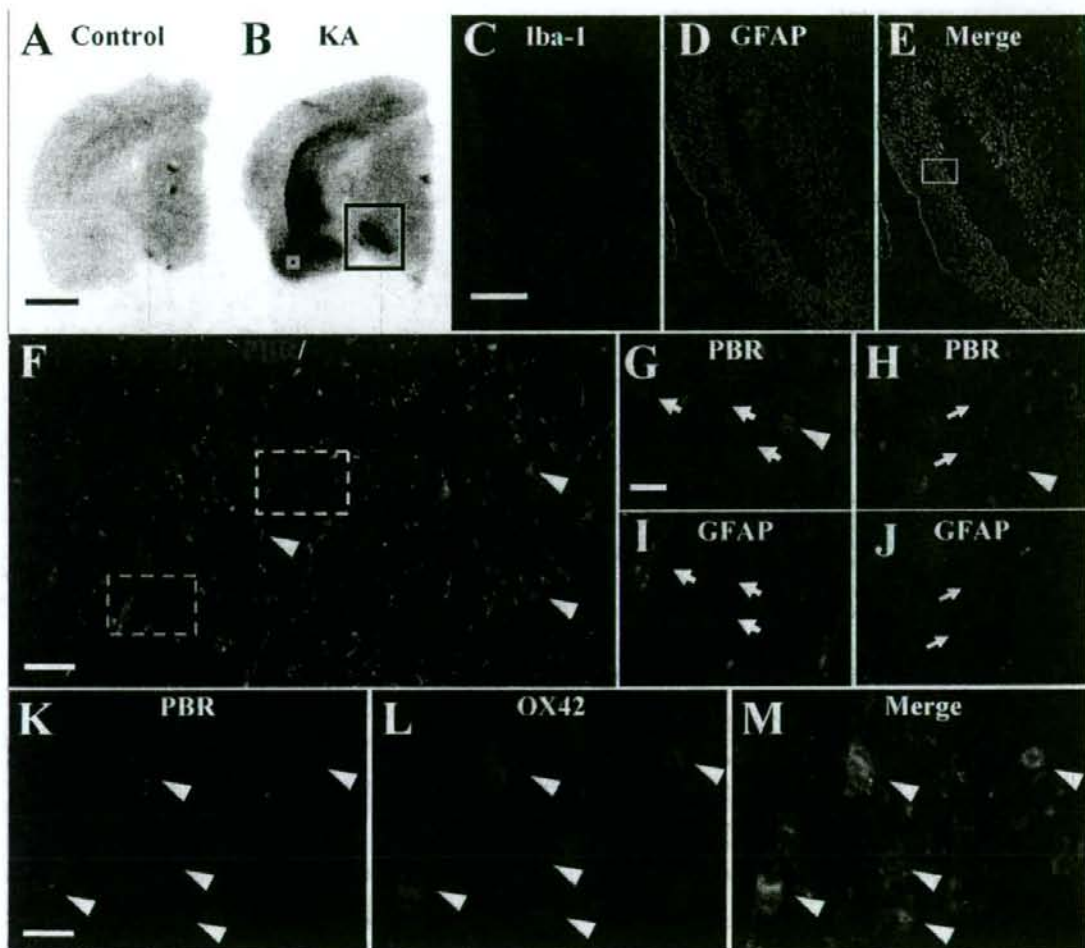
Figure 3. *A, B,* Autoradiographic labeling of PBR in brain sections of untreated control (*A*) and KA-treated (*B*) rats. Black square indicates intense radiolabeling with [¹⁸F]FE-DAA1106 in the midbrain, and immunolabeling of gliotic changes in this area is shown in *C–E* at high magnification. High-power photomicrographs of the entorhinal area indicated by yellow square in *B* are also shown in *K–M* for the purpose of clarifying the cellular localization of PBR. *C–E,* Double immunofluorescence labeling of Iba-1 (*C*) and GFAP (*D*) along with two-channel image (*E*) in the midbrain of KA-treated rat. The section is subadjacent to the sample shown in *B*. The square indicates a subregion with marked astrogliosis shown in *F* at high magnification. *F–J,* Midbrain of KA-treated rat doubly labeled with NP155 (*F–H;* green) and anti-GFAP (*F, I, J;* red) antibodies. Broken yellow and white lines delineate areas presented in *G* and *I* and *H* and *J,* respectively, at high magnification. The majority of astrocytes did not exhibit PBR signals at a visible level (arrows in *G, I*), whereas a small subset of GFAP labeling overlapped with weak PBR immunoreactivity (arrows in *H, J*). Round-shaped PBR immunolabeling (arrowheads in *G, H*) was not colocalized with GFAP staining and was conceived to be microglial. *K–M,* Double immunolabeling for PBR (*K*) and CD11b (*L*) illustrating speckled PBR staining (arrowheads) packed in microglia (2-channel image shown in *M*). Scale bars: (*A, B*) 2 mm, (*C–E*) 500 μm, (*F*) 40 μm, (*G–J*) 20 μm, (*K–M*) 10 μm.

cally (mean ± SE, 100.0 ± 3.6% vs 100.8 ± 6.8% of contralateral mean for contralateral vs ipsilateral striata; $p > 0.05$ by t test; $n = 4$ per group) detectable elevation of PBR levels. Similarly, the intensity of PBR radiolabeling in the striatum of MPTP-treated marmosets did not significantly differ from that of untreated controls (mean ± SE, 100.0 ± 4.4% vs 84.8 ± 4.2% of control for control vs MPTP-treated groups; $p > 0.05$ by t test; $n = 5$ per group), notwithstanding the severe impairments of striatal dopaminergic terminals (Ando et al., 2008). Together, these findings demonstrate that astroglial PBR in the striatum is not upregulated when the injury provokes no significant activation of striatal microglia.

Demyelinating but reversible pathology of the striatum leading to synergistic activation of astrocytes with high-level PBR and microglia with low-level PBR

On the assumption that PBR-positive astrocytes and PBR-negative microglia may reflect reversible neuropathological processes, we investigated mice at a subchronic stage of treatment with copper chelator cuprizone (CZ), which is known to induce recoverable loss of myelin (Chen et al., 2004). Oral administration of cuprizone for 4 weeks resulted in concentrations of PBR in the striatum and corpus callosum (Fig. 5A) (mean ± SE, 100.0 ± 13.2% vs 216.6 ± 1.9% of control for control vs CZ-treated striata; $p < 0.01$ by t test; $n = 3$ per group), which were spatially
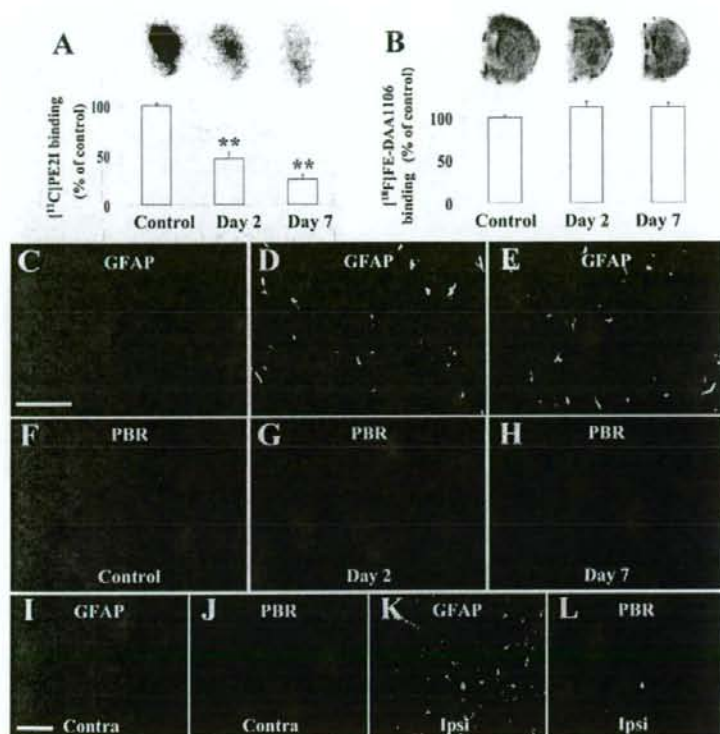
Figure 4. *A, B,* Autoradiographic analyses of dopamine transporter (*A*) and PBR (*B*) in striatal regions of mice without treatment and 2 and 7 d after initiation of METH treatment (*n* = 6 per group). Significant decline of [^{11}C]PE2I binding to dopamine transporter was observed after METH administration (**$p < 0.01$ by Bonferroni's multiple comparison after ANOVA), whereas changes in binding of [^{18}F]FE-DAA1106 to PBR were insignificant ($p > 0.05$ by ANOVA). Error bars represent SE. Representative autoradiograms are displayed on top. *C–H,* Double immunofluorescence staining with anti-GFAP antibody (*C–E*) and NP155 (*F–H*) in striatal sections of mice without treatment (left) and 2 (middle) and 7 (right) d of METH challenge. *I–L,* Double immunofluorescence staining with anti-GFAP antibody (*I, J*) and NP155 (*K, L*) in contralateral (left column) and ipsilateral (middle column) striata of 6-OHDA-treated rats. Error bars in graphs represent SE. Scale bars, (*C–L*) 75 μm.

consistent with abundant accumulations of GFAP-positive astrocytes and Iba-1-positive microglia (Fig. 5*B–E*). The Iba-1 immunostaining in the striatum was intensified in patchy clusters (Fig. 5*E*), and double immunolabeling for MBP and Iba-1 illustrated that these clusters were composed of activated microglia associated with destroyed myelinated fibers (Fig. 5*F*). Unlike microglial activation, astrogliosis was not confined to the site of demyelination (Fig. 5*G*). As seen in a low-power image (supplemental Fig. 1*G*, available at www.jneurosci.org as supplemental material), NP155-labeled PBR signals were diffusely distributed in the striatum of cuprizone-treated mice, which resembled the spatial profile of activated astrocytes and was in clear contrast to the microgliosis locally restricted to demyelinated fiber bundles. At a high magnification, the vast majority of astrocytes exhibited distinct upregulation of PBR, and PBR signals were almost exclusively present in the astroglial compartment (Fig. 5*H*).

We then conducted *in vivo* detection of PBR in these mice by using microPET and [^{18}F]FE-DAA1106 to clarify the detectability of astroglial PBR in living brains. CZ-treated mice showed a profoundly increased concentration of radiotracer in the striatal area (Fig. 5*I,J*), ~2-fold that in control mice (Fig. 5*K*), corresponding well with the *in vitro* autoradiographic data (Fig. 5*A*).

Thus, our findings provide the first clear evidence for the ability of PET and specific radioligand to capture PBR upregulation in astrocytes.

Induction of astroglial PBR by transplantation of immortalized microglia

The mechanistic links between activated microglia and PBR expression in astrocytes were assessed by immunohistochemically assaying PBR levels in the mouse hippocampus transplanted with the PKH26-labeled immortalized microglial cell line, Ra2 (Fig. 6*A*), which has been shown to be neuroprotective and reactive oxygen species- (ROS) nonproducing (Sawada et al., 2006). Compared with the vehicle-injected side (Fig. 6*B–E*), the Ra2-injected hippocampus exhibited astrocytes with hypertrophic morphology in close proximity to the grafted microglia, and a high-level expression of PBR was observed in these astrocytes (Fig. 6*F–I*). Compared with the vehicle-injected side (Fig. 6*J*), pronounced activation of resident (Iba1-positive, PKH26-negative) microglia was found in the proximity of the transplanted (PHK-positive) Ra2 cells (Fig. 6*K–M*). As PBR signals showed nearly complete overlap with GFAP immunoreactivity in this area, these activated endogenous microglia were presumed to be PBR-negative. Neuronal damage and loss of myelin were negligible in these areas. Because the hippocampal subregions analyzed here were sufficiently distant from needle tracks (Fig. 6*A*) and were consequently little affected by traumatic insults, these data demonstrate that activated microglia without evident neurotoxicity can act as the sole initiator of PBR upregulation in nearby astrocytes, and imply the presence of mechanistic links between activations of PBR-negative endogenous microglia and PBR-positive astrocytes.

Augmented GDNF expression in PBR-positive astrocytes

To supplement the evidence for the protective and restorative roles of PBR-expressing astrocytes, we immunohistochemically examined astroglial GDNF in the experimental models beside those of AD. Double fluorescence staining for control rodents illustrated the expression of GDNF in resident astrocytes at a moderate level in the hippocampus (Fig. 7*A,B*, insets) and at a very low level in the striatum (Fig. 7*E,F,I,J*) and midbrain (Fig. 7*M,N*) of mice and rats. A notable increase of astroglial GDNF immunoreactivity was found in the Ra2-transplanted hippocampus (Fig. 7*C,D*) and CZ-treated striatum (Fig. 7*G,H*), in which remarkably upregulated PBR in astrocytes was featured. Striatal astrocytes reacting to injuries of dopaminergic terminals exhibited no substantial increase in GDNF levels (Fig. 7*K,L*), in concordance with the unaltered PBR signals. Activated astrocytes in the midbrain subregion surrounding inflammatory microglia also did not express GDNF at a clearly detectable level (Fig. 7*O,P*),